CHEMISTRY OF MATERIALS

pubs.acs.org/cm

Article

Anion and Cation Size Effects on Viscoelasticity and Ion Transport of Imine Vitrimer Electrolytes

Seongon Jang, Ruey-Bin Tsai, Charles M. Schroeder, and Christopher M. Evans*

Cite This: *Chem. Mater.* 2025, 37, 7037−7048

Read Online

ACCESS | Metrics & More | Article Recommendations | Supporting Information

ABSTRACT: Vitrimers are a subclass of covalent adaptable networks where bond exchange occurs without breaking, thereby offering polymer materials with enhanced mechanical strength, thermal stability, and reprocessability compared to conventional electrolytes. Despite recent progress, we lack a complete understanding of the role of ions in controlling the physical and chemical properties of vitrimers. In this work, we study how different salts affect the viscoelasticity, morphology, and ionic conductivity of imine vitrimers. Our results show that addition of salt decreases relaxation times at elevated temperatures due to the catalytic effect of the cations, with smaller cations leading to faster relaxation. However, the activation energy for terminal relaxation increases with smaller cation size. This apparent discrepancy is attributed to the complex interplay among bond exchange kinetics, chain diffusion, and salt dissociation. Anions act as plasticizers by reducing the shear modulus, except lithium bromide. Ionic conductivity increases with larger anions due to smaller salt dissociation energies, whereas the cation type has a minor impact as polymer segmental dynamics dominate ionic transport. Imine-based vitrimers are reprocessable and recyclable, maintaining original mechanical properties and ionic conductivity after recovery. Mixed salt vitrimers exhibited tunable viscoelasticity and ionic conductivity intermediate to the analogous pure salt systems. Overall, this work highlights the role of salt in the dynamic and conductive properties of imine vitrimers.

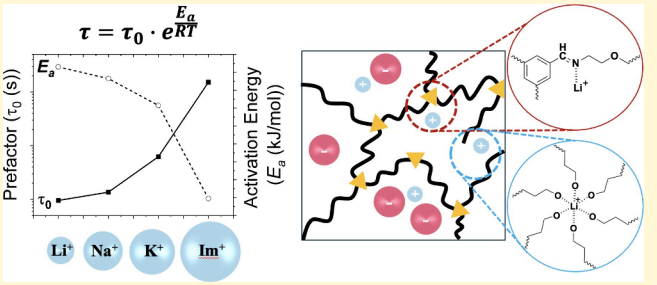

INTRODUCTION

The increasing demand for next-generation energy storage devices motivates the need for new materials to address the stability and safety challenges associated with potentially toxic liquid electrolytes.[1,2] Although liquid electrolytes have been extensively investigated, they possess inherent drawbacks such as the use of volatile, flammable organic solvents and the risk of leakage.[3] To mitigate these concerns, solid-state electrolytes (SSEs) including inorganic and organic materials offer promising alternatives due to their high energy density, mechanical robustness, and thermal stability.[4] However, inorganic SSEs are hindered by their mechanical brittleness and substantial interfacial resistance between the electrode and electrolyte.[5] In contrast, solid polymer electrolytes (SPEs) offer advantages in terms of facile processing and mechanical flexibility, which improves interfacial contacts and reduces interfacial resistance.[6,7]

Poly(ethylene oxide) (PEO) is one of the most extensively studied polymers for SPEs due to its electrochemical and chemical stability. The physical and chemical properties of PEO-based electrolytes have been thoroughly explored since the 1970s.[8−10,12−14] It is well-established that lithium ions (Li^+) interact with PEO via chelating complexation with oxygen atoms in the polymer backbone.[14] However, the high degree of PEO crystallinity results in low ionic conductivity at room temperature, limiting practical applications. Several strategies have been attempted to suppress the crystallization of PEO chains such as covalent cross-linking, which improves mechanical and thermal stability.[8,11] In addition, cross-linked PEO electrolytes can effectively suppress lithium dendrite formation due to their nanoscale mesh size.[11] However, permanent covalent networks are difficult to reprocess or recycle after curing, and dendrite formation nevertheless occurs, which decreases the performance lifetime of these materials.[8]

Vitrimers have received significant attention and exhibit properties ranging from thermoset-like rigidity to thermoplastic-like reprocessability depending on cross-linking density,[16] exchange kinetics,[17] and polymer backbone chemistry.[18] This versatility has led to the use of vitrimers in several applications, including 3D printing,[19] self-healing materials,[20] shape-memory materials,[21,22] actuators,[23,24] shockwave dissipation,[25,26] and SPEs.[27−29] Among several applications, vitrimers have emerged as a promising route for electrolytes,

Received: April 23, 2025
Revised: August 18, 2025
Accepted: August 20, 2025
Published: September 3, 2025

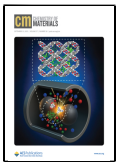

https://doi.org/10.1021/acs.chemmater.5c00991
Chem. Mater. 2025, 37, 7037−7048

offering the potential for self-healing, reprocessability, and recyclability. In vitrimer electrolytes, dissociated ions can interact with both dynamic covalent bonds and polymer backbones.[28] Although this complex interplay impacts both conductivity and viscoelasticity of vitrimers, ion−polymer interactions have not yet been extensively studied for a broad range of salts.

Prior work showed that cations and anions from lithium bis(trifluoromethane) sulfonimide (LiTFSI) salts coordinate with vinylogous urethanes (VU)[28] and boronic esters,[30,31] respectively, in ethylene oxide (EO)-based vitrimers. As the EO length decreases, Li^+ tends to coordinate with VU bonds as short EO chains are not able to effectively solvate Li^+, demonstrated by ^7Li solid-state NMR experiments. Computational modeling using density functional theory (DFT) further supports the change in the Li^+ environment with EO length, which leads to changes in viscoelasticity, reprocessability, and ionic conductivity.[28] Prior work also has shown that Li^+ acts as Lewis acid catalysts for VU bonds, which accelerates bond exchange and facilitates reprocessing compared to neutral vitrimers.[27−29] This effect is more pronounced for short EO chains where the Li^+ prefers to coordinate with VU. In boronic ester vitrimers, the dynamic bond is a Lewis acid and coordinates with the anion TFSI. Upon increasing the concentration of LiTFSI salt, the shear modulus significantly decreases due to an effective reduction in cross-link density.[30,31] Boronic esters can also be converted to anionic boronates by adding lithium hydroxide (LiOH), in which case Li^+ coordinates with the dynamic bond.[56]

Prior work has investigated ion-specific effects in polymer electrolytes without dynamic bonds such as linear and cross-linked PEO electrolytes using experimental[32−35] and computational[36,37] approaches. Nanthana and co-workers focused on understanding how different anions affect Li^+ conduction in poly(ethylene carbonate) electrolytes, showing that larger anions such as TFSI enhance Li^+ transport.[32] Jeschull and co-workers examined the role of cation size in the thermal and ion transport properties of PEO block copolymer-based electrolytes (PEO-BPE) using different cations (Li^+, Na^+, and K^+) with TFSI anions.[34] Aside from linear PEO-based electrolytes, Braun and co-workers explored how ion size affects ion transport in solvent-free cross-linked PEO networks above their glass transition temperatures (T_g), revealing that larger counteranions selectively enhance Li^+ transport.[35]

In recent years, imine bonds have garnered significant attention due to their potential use in SPEs. Imine bonds generally show more rapid exchange kinetics compared to VU bonds and are more stable than boronic esters.[38−45] Wang and colleagues showed that imine vitrimer electrolytes exhibit higher ionic conductivity than linear or permanently cross-linked PEO electrolytes.[43] Fang and co-workers successfully synthesized soy protein-based imine dynamic network electrolytes that demonstrated their recyclability at room temperature.[44] A previous study by Zhou and co-workers revealed that incorporating three different salts (LiFSI, KFSI, and KPF_6) into vinylogous urethane vitrimers enables control over their mechanical, viscoelastic, and thermal properties.[29] Despite recent progress, we lack a complete understanding of the role of different ionic species in the properties of dynamic covalent polymer networks such as imine vitrimers.

In this work, we study the influence of different ions on the viscoelasticity, morphology, and ion transport properties of imine vitrimers using oscillatory shear rheology, wide-angle X-ray scattering (WAXS), and electrochemical impedance spectroscopy (EIS). A series of imine vitrimers with six different salts was prepared to probe the role of ion size in material properties. Rheological measurements indicate that added salt accelerates the terminal relaxation times of the vitrimers, which is attributed to the catalytic effect of cations on imine bond exchange. However, the temperature dependence of relaxation times for imine vitrimers varied with ion size, which is attributed to the combined influence of ion−polymer interactions, ion−imine interactions, and salt dissociation. In contrast to the terminal relaxation times, the ionic conductivity of imine vitrimers with different anions ($TFSI^-$, OTf^-, and Br^-) but the same cation (Li^+) increases with larger anions due to lower salt dissociation energies. The ionic conductivity of vitrimers containing TFSI salts with different cations (Li^+, Na^+, K^+, and Im^+) is primarily dominated by segmental dynamics and can be normalized by T_g. The shear modulus of vitrimers decreases with the addition of salts containing larger anions due to their plasticizing effect on PEO chains, supported by X-ray scattering analysis. In all cases, vitrimers can be successfully reprocessed into micrometer-thick films by applying heat and pressure. Moreover, these networks can be fully de-cross-linked into linear PEO chains and cross-linkers and subsequently repolymerized into networks upon solvent removal, thereby demonstrating their recyclability. Vitrimer properties can also be controlled by addition of multiple salts, where ionic conductivity and modulus show additive behavior relative to the pure salt analogs. Overall, this work provides an improved understanding of the role of ion selection in the physical and ion conducting properties of imine vitrimers.

EXPERIMENTAL PROCEDURES

Materials. Poly(ethylene glycol) diamine (PEG-NH_2, average M_n = 2000 g/mol), lithium bis(trifluoromethanesulfonyl)imide (LiTFSI, 99%), lithium bromide (LiBr, 99%), lithium trifluoromethanesulfonate (LiOTf, 99.995%), and acetonitrile (anhydrous, 99.8%) were purchased from Sigma-Aldrich. Sodium bis(trifluoromethanesulfonyl)imide (NaTFSI, 98%), 1-ethyl-3-methylimidazolium bis(trifluoromethanesulfonyl)imide (ImTFSI, 98%), and potassium bis(trifluoromethanesulfonyl)imide (KTFSI, 98%) were purchased from TCI America. Benzene-1,3,5-tricarbaldehyde (BTA, 97%) was purchased from Combi-Blocks. Ethanol (anhydrous, UPS Specs) was purchased from Decon Laboratories, Inc. Distilled water was obtained from a Synergy water purification system. All chemicals were used without further purification.

Synthetic Procedures. *Dynamic Network Synthesis.* In an Ar glovebox, poly(ethylene oxide)-diamine (PEO-NH_2, 3.3 eqv) and benzene-1,3,5-tricarbaldehyde (BTA, 2 eqv) were weighed into a 20 mL vial. The ratio of amine to aldehyde groups was 1.1:1. Next, salts (ratio of cation and ethylene oxide repeat units $r = \frac{[M^+]}{[EO]} = 0.05$ for all vitrimers, M^+ = Li^+, Na^+, K^+, and Im^+) were added to the vial and removed from the glovebox. After adding 2.5 mL of acetonitrile into the vial, the mixture was vigorously mixed using a vortex mixer for 15 s and then a sonicator bath for 15 min. The solution was transferred to a Teflon dish, and the resulting mixture was cured at 30 °C for 2 h under ambient conditions. The polymer network was further dried at 50 and 80 °C for 24 h at each temperature under vacuum to remove water and promote high conversion, resulting in yellow or dark yellow-colored films (Figure S1). All samples were stored in the glovebox before further characterization. Neutral vitrimer networks were synthesized using the same procedure without adding salts.

Attenuated Total Reflectance-Fourier Transform Infrared Spectroscopy (ATR-FTIR). Infrared spectra were obtained using a Bruker ALPHA FTIR spectrometer with a platinum-ATR QuickSnap sampling module. All samples were measured at 100 °C to ensure

https://doi.org/10.1021/acs.chemmater.5c00991
Chem. Mater. 2025, 37, 7037−7048

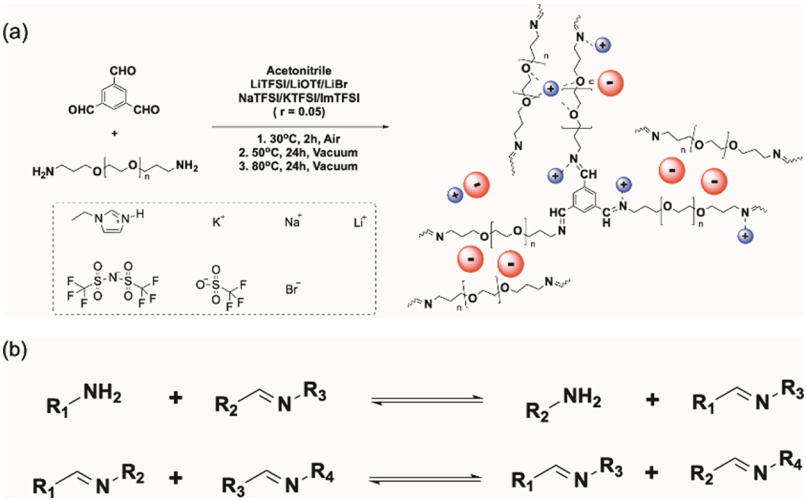

Figure 1. Synthesis and preparation of imine vitrimers. (a) Reaction scheme for the formation of imine vitrimers with and without salt. Dissociated ions interact with both imine bonds and ether oxygen atoms of PEO chains. (b) Two mechanisms of imine bond exchange, including transamination and imine metathesis.

good contact between the samples and the window. The range of scanning was from 4000 to 400 cm^{-1} with 32 scans and a 4 cm^{-1} resolution.

Solution-Phase NMR. ^1H spectra were obtained on a Caliver Bruker 500 MHz NMR spectrometer using $CDCl_3$ as the reference solvent.

Differential Scanning Calorimetry (DSC). DSC measurements were performed by a TA Instruments DSC 2500. Samples were sealed in Tzero aluminum pans inside a Ar glovebox. Subsequently, the samples were subjected to a heat/cool/heat cycle in a temperature range from −100 to 100 °C with 10 °C/min for all samples. The glass transition temperature T_g was determined using the 1/2 ΔC_p criterion from the second heating cycle.

Thermogravimetric Analysis (TGA). The thermal stability of the polymer samples was assessed by a TA Instruments Q50. Each sample was heated from 30 to 600 °C at a rate of 10 °C/min under N_2.

Electrochemical Impedance Spectroscopy (EIS). Impedance measurements were performed using a Biologic SP300 potentiostat with a controlled environment Sample holder and intermediate temperature system accessories. Impedance spectra were collected by applying an AC potential of 20 mV from 1 MHz to 100 mHz. The real conductivity (σ') was calculated from complex impedance, $Z^* = Z' + i\omega Z''$ based on the equation:

$$\sigma'(\omega) = \frac{l}{A} \times \frac{Z'(\omega)}{[Z'(w)^2 + Z''(w)^2]}$$

where l is thickness of the film, A is the film surface area, and ω is the frequency. All samples were prepared with CR2032 coin cells that were assembled following a previous literature protocol.[30] Temperature-dependent impedance measurements were performed from 95 to 25 °C with 5 °C steps after reaching the thermal equilibrium state at the highest temperature.

Wide-Angle X-ray Scattering (WAXS). The morphology of the vitrimers was characterized using a Xenocs GeniX3D Cu Kα X-ray source (1.54 Å) with a Pilatus 2D detector. A road beam stop is positioned in front of the detector to dampen the primary beam. The sample-to-detector distance was calibrated using silver behenate powder. To prevent the samples from exposure to moisture, the samples were packed in a 1 mm-thick quartz capillary tube under an Ar environment and sealed with marine epoxy (Devcon, home 5 min Epoxy). All measurements were collected under ambient conditions with a 30 min exposure time. The 2D diffraction data were processed using FIT2D software to obtain plots of intensity versus scattering vector.

Rheology. Rheological characterization was performed using a TA Instruments DHR-2 outfitted with an environmental control chamber and 8 mm or 4 mm diameter stainless-steel parallel plates. Before each measurement, samples were prepared into a circular geometry of 10 mm diameter using a Teflon washer at 130 °C by applying 5 kg weights overnight in an Ar glovebox. The samples were then loaded onto the rheometer plates preheated at 130 °C. The thickness of samples ranged between 800 and 900 μm. Experiments were collected in the linear regime based on strain sweep measurements from 0.1 to 5% for all samples at the highest temperature. Dynamic oscillatory linear viscoelastic (LVE) experiments were measured from 100 to 0.01 rad/s and from 130 to 70 °C with 10 °C steps. Temperature ramps were performed by heating from 70 to 130 °C at a rate of 2 °C/min at 1 Hz. The characteristic relaxation time (τ) was defined where the shear storage (G') and loss (G'') moduli have the same value. These relaxation times were plotted as a function of $1000/T$ and fit to an Arrhenius equation. The activation energy for flow was determined in each sample from the slope. Stress relaxation experiments were conducted in the linear regime (γ = 1%) from 130 to 20 °C with 10 °C steps. The characteristic relaxation time (τ) was extracted using double Maxwell model fitting.

Reprocessing (Thermal Method). A mixed salt (LiTFSI and LiBr) vitrimer was prepared by using the same synthetic procedures, except that each salt concentration was fixed at $r = \frac{[M^+]}{[EO]} = 0.025$ to match the total salt concentration of the other salt vitrimers. To demonstrate reprocessability, the mixed salt vitrimer was broken into small pieces and hot pressed into smooth films by applying 3 tons of pressure for 20 min at 130 °C. Then, the vitrimer film was measured by a rheometer and the reprocessing was repeated up to five times.

Recycling (Solvent Method). A vitrimer network with KTFSI salts was added to a mixture of ethanol (2 mL) and distilled water (0.5 mL). Then, the mixture was stirred at room temperature overnight. The vitrimer was recovered by heating at room temperature (1.5 h) and 60 °C (3.5 h), followed by vacuum drying at 60 and 110 °C for 24 h at each temperature to remove any residual solvent. After processing into films, the samples were measured with a rheometer and electrochemical impedance spectroscopy as described in the Rheology and Electrochemical Impedance Spectroscopy (EIS) sections.

RESULTS AND DISCUSSION

Design, Synthesis, and Structural Characterization of Imine Vitrimers. Imine vitrimers were prepared by a Schiff base reaction between benzene-1,3,5-tricarbaldehyde and

https://doi.org/10.1021/acs.chemmater.5c00991
Chem. Mater. 2025, 37, 7037−7048

Table 1. Thermal Transitions, Shear Moduli, Terminal Relaxation Times, Activation Energies, and Ion Conductivities of Imine Vitrimers

sample	T_g (°C)[a]	T_m (°C)[a]	$T_{d,95\%}$ (°C)[b]	G' (MPa)[c]	$\tau_{130\ °C}$(s)	$\tau_{90\ °C}$(s)	E_a (kJ/mol)[d](R^2)	τ_0 (s)	$\sigma_{90\ °C}$ (S/cm)	$\sigma_{25\ °C}$ (S/cm)
neutral	−36[e]	31	358	2.1	19.3	85.2	32.8 (0.996)	1.19×10^{-3}		
LiTFSI	−45	21	364	1.1	6.3	50.5	60.6 (0.998)	9.53×10^{-8}	4.04×10^{-4}	2.44×10^{-5}
NaTFSI	−45	25	352	1.2	6.5	47.6	59.3 (0.994)	1.36×10^{-7}	9.70×10^{-4}	2.49×10^{-5}
KTFSI	−48		358	1.0	11.6	74.9	56.3 (0.990)	6.21×10^{-7}	1.24×10^{-3}	2.76×10^{-5}
ImTFSI	−55	26	340	1.1	11.5	62.4	45.9 (0.999)	1.52×10^{-5}	9.24×10^{-4}	6.00×10^{-5}
LiOTf	−46	30	359	1.5	5.5	34.5	54.5 (0.999)	4.86×10^{-7}	3.70×10^{-4}	1.17×10^{-5}
LiBr	−46[e]	34	337	3.6	6.4	29.9	44.1 (0.990)	1.34×10^{-5}	9.15×10^{-5}	6.68×10^{-6}

[a]Determined from second heating DSC curves. [b]TGA onset temperatures after 5% weight loss. [c]Obtained from a rubbery plateau of frequency sweep experiments (10 rad/s, 130 °C). [d]Determined from the slope of Arrhenius plots. [e]Determined from DSC cooling curves instead of second heating curves due to PEO chain crystallization.

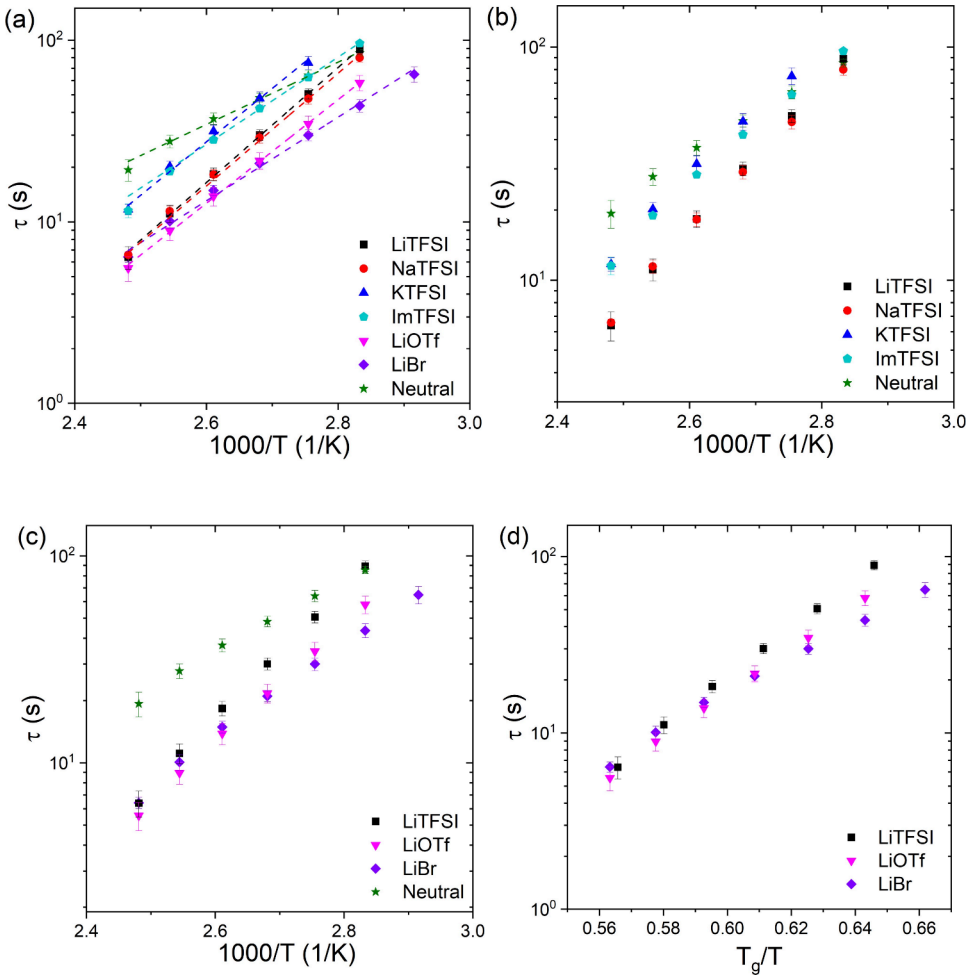

Figure 2. Relaxation dynamics of imine vitrimers. (a) Arrhenius plots of the imine vitrimers indicate that the addition of salts leads to shorter characteristic relaxation times τ compared to the neutral vitrimers, which is attributed to the catalytic effect of cations on imine bond exchanges. Dashed lines represent Arrhenius fits. (b) Imine vitrimers with smaller cations exhibit a stronger temperature dependence on relaxation times, indicating larger activation energy E_a. (c) Imine vitrimers with smaller anions display a weaker temperature dependence of relaxation times (lower E_a) compared to the neutral vitrimer. (d) T_g-normalized Arrhenius plot of the imine vitrimers with different anions but the same cation, demonstrating that their viscoelastic properties are coupled with segmental dynamics.

amino-terminated poly(ethylene oxide) ($\bar{M}_n$ = 2000 g/mol). For ionically conductive vitrimers, lithium bis(trifluoromethanesulfonyl)imide (LiTFSI), lithium trifluoromethanesulfonate (LiOTf), lithium bromide (LiBr), sodium bis(trifluoromethanesulfonyl)imide (NaTFSI), potassium bis(trifluoromethanesulfonyl)imide (KTFSI), or 1-ethyl-3-methylimidazolium bis(trifluoromethanesulfonyl)imide (ImTFSI) was added to the reaction mixture before polymerization (Figure 1 and Supporting Information, SI). The properties of vitrimers are modified by addition of salt,[27,28,30] quantified by the ratio r of salt to ethylene oxide repeat units ($r = \frac{[M^+]}{[EO]}$). Attenuated total reflectance-Fourier transform infrared spectroscopy (ATR-FTIR), differential calorimetry scanning (DSC), thermogravimetric analysis (TGA), rheometry, and electrochemical impedance spectroscopy (EIS) (Figures S2–

https://doi.org/10.1021/acs.chemmater.5c00991
Chem. Mater. 2025, 37, 7037−7048

S6) were used to characterize vitrimer properties as a function of salt concentration. Upon increasing LiTFSI concentration, the relaxation times and shear modulus plateau values decreased, which is attributed to the catalytic effect of Li^+ on imine bond exchange[15,59] and the plasticizing effect of TFSI anions,[28,29] respectively. A salt concentration of $r = 0.05$ resulted in vitrimers with a shear modulus plateau (G') above 1 MPa, which can effectively suppress lithium dendrite growth.[11] In addition, their small characteristic relaxation times τ and high ionic conductivities σ enabled facile processing and rheological measurements.

Following polymerization, the formation of imine bonds in all samples was confirmed using ATR-FTIR by the appearance of the imine peak at 1640 cm^{-1} (Figure S7). In addition, TGA showed negligible mass loss below 300 °C, confirming the complete elimination of water during polymerization and high conversion of the polymer networks (Figure S8). Degradation temperatures $T_{d,95\%}$ were consistent with values reported in prior work (Table 1).[38,43,44] DSC was performed to examine the thermal transitions in the temperature range between −100 and 100 °C (Figure S9), and the T_g and T_m values are summarized in Table 1. In neutral vitrimers, a distinct melting transition during the second heating cycle was observed at 31 °C due to the crystallization of long PEO chains. The melting temperatures T_m diminished or disappeared upon addition of salt (Figure S9), which is attributed to the plasticizing effect of TFSI anions on PEO chains.[28,29] Smaller cations led to higher T_g values. This trend may result from their greater charge density, which promotes stronger interactions with ether oxygen atoms along PEO backbones and restricts segmental dynamics.[46,47] Vitrimers containing salts exhibited lower T_g values compared to neutral vitrimers (Table 1), which may arise from the plasticizing effect of the anions and reduced crystallinity.[28,29] Notably, the enthalpy of fusion for LiBr vitrimers significantly decreased relative to neutral vitrimers (Figure S9b), indicating reduced crystallinity or fewer crystallites acting as physical cross-links. This reduction in crystallinity also enhanced chain mobility, as supported by a decrease in T_g. Although the LiBr vitrimer displayed a slightly higher T_m, with an increase of less than 3 °C compared to the neutral vitrimer, this modest T_m elevation may result from strong association between Br^- and PEO chains, as demonstrated in PEO electrolytes containing halides via molecular dynamics simulations.[36] Nonetheless, such interactions are likely confined to the interfacial regions of crystallites, as plasticizers or additives generally do not penetrate the densely packed crystalline domains.[68]

Effect of Different Salts on Viscoelasticity of Imine Vitrimers. Small amplitude oscillatory shear (SAOS) rheology experiments were performed to characterize the linear viscoelastic properties of imine vitrimers across a range of temperatures (SI). Characteristic relaxation times τ were obtained from the reciprocal of the crossover frequency ω_c at which the storage modulus G' equals the loss modulus G''. In Figure 2a, τ is plotted as a function of inverse absolute temperature, showing an Arrhenius dependence of relaxation times for all samples. The characteristic relaxation times of the salt-containing vitrimers decreased compared to the neutral vitrimer at temperatures above 100 °C, and the effect was the most pronounced for Li salts. Previous studies have reported that Li^+ accelerates bond exchange kinetics by acting as a Lewis acid catalyst in vinylogous urethane vitrimers.[27−29] Ciaccia and Di Stefano investigated the mechanisms of imine exchange reactions in organic solvents, revealing that Lewis acid catalysts such as Sc(III) or molybdenum complexes catalyze transamination (amine−imine exchange) and imine metathesis, respectively.[15] We hypothesize that salts accelerate bond exchange by acting as Lewis acid catalysts, facilitating the reaction when imine bonds encounter each other via chain diffusion, thereby leading to smaller relaxation times. This catalytic effect depends on the specific interactions between imine bonds and cations (Li^+, Na^+, K^+, and Im^+), with Li^+ showing the strongest effect. The activation energy E_a for relaxation times was obtained by fitting experimental data to eq 1 (Arrhenius equation):

$$\tau = \tau_0 \exp\left(\frac{E_a}{RT}\right) \quad (1)$$

where τ_0 is a numerical prefactor (Table 1). The prefactor in eq 1 can be interpreted as the characteristic relaxation time at infinite temperature, where the energy barrier for bond exchange is negligible. Interestingly, all salt vitrimers exhibit higher E compared to the neutral vitrimer. If the relaxation process of vitrimers is primarily governed by bond exchange reactions, then this trend between τ and E_a may appear counterintuitive.[48,49] However, similar observations have been reported in dynamic polyesters[16,50] and vinylogous urethane vitrimers.[29,66] To explain this apparent discrepancy, recent studies emphasize the importance of considering both chain diffusion and bond exchange kinetics.[51−53,58] For example, Hayashi and Isogai demonstrated that cross-linking density significantly affects both E_a and τ, as highly cross-linked structures restrict chain diffusion, hindering the effective occurrence of dynamic bond exchange.[51] Furthermore, incorporation of catalytic species can introduce additional complexity, particularly when their activity exhibits strong temperature dependence. Du Prez and co-workers showed that Brønsted acids in vinylogous urethane vitrimers substantially accelerate dynamics at elevated temperatures by generating more catalytically active species. In contrast, the neutral form of acids restricts chain diffusion at lower temperatures.[66] This strong temperature dependence of catalytic species leads to higher E_a energies yet faster τ at high temperatures. Likewise, salts in our vitrimers dissociate into ions that interact with dynamic bonds and polymer backbones, with their dissociation varying with temperature.[67] As a result, E_a measured by rheology can appear higher even when τ decreases at elevated temperatures due to the combined contributions of both chain diffusion and bond exchange kinetics.

Characteristic relaxation times showed a trend with cation size (Figure 2b and Figure S10). Vitrimers with smaller cations exhibited smaller τ and τ_0 values due to stronger Lewis acidity, resulting in an increased catalytic effect on imine bond exchange.[46] However, the trend of τ is not universal and appears to vary with temperature due to factors, such as the salt dissociation degree, imine bond exchange kinetics, and segmental dynamics, all of which are influenced by temperature changes (Figure S10a). Interestingly, when replotted as T_g/T, a monotonic trend is observed where smaller cations show smaller τ values (Figure S10b). This suggests that the stronger catalytic effect of smaller cations governs bulk relaxation rather than segmental dynamics and salt dissociation within this temperature window. In contrast, E_a values increased with smaller cations, indicating that τ depends more strongly on temperature for smaller cations (Table 1).

https://doi.org/10.1021/acs.chemmater.5c00991
Chem. Mater. 2025, 37, 7037−7048

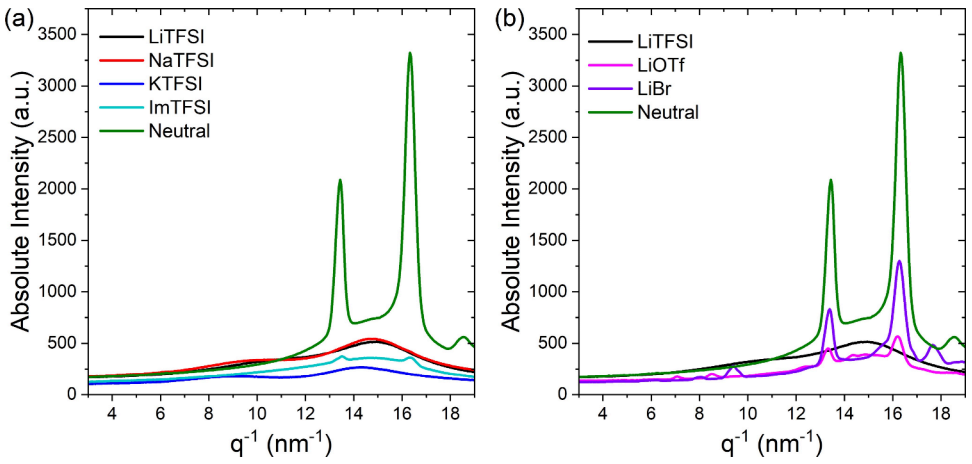

Figure 3. Wide-angle X-ray scattering (WAXS) patterns for imine vitrimers with different salts. (a) Vitrimers with different cations but the same anion. All cation vitrimers exhibit broad amorphous halo peaks, attributed to the plasticizing effect of TFSI anions. (b) Vitrimers with different anions but the same cation. OTf and Br anions partially suppress the crystallization of PEO chains with weaker peaks at the same locations as in the neutral vitrimer.

The interactions between ions and polymer backbones, as well as between ions and imine groups, are both temperature-dependent and likely influencing E_a values in salt-containing vitrimers. Smaller cations promote stronger interactions with polymer backbones due to their high charge density, likely slowing down chain diffusion to a greater extent upon cooling. As a result, the relaxation times become more temperature-dependent, represented by higher E_a.

Salt vitrimers with different anions ($TFSI^-$, OTf^-, and Br^-) but the same cation (Li^+) also exhibited faster relaxation behavior than neutral vitrimers (Figure 2c). However, smaller anions led to increased τ_0 and decreased E_a, which is attributed to the difference in salt dissociation energy (Figure S12 and Table S1). Previous studies showed that the dissociation energy of salts increases with smaller cations and anions in polymer electrolytes (Table S1).[35,54,55,63−65] Additionally, coarse-grained molecular dynamics simulations were used to capture size-dependent solvation effects of salts in polymer electrolytes, demonstrating that larger anions result in nearly full ion dissociation.[37] LiTFSI has the lowest dissociation energy, leading to more dissociated Li^+ serving as Lewis acid catalysts for imine bond exchange in the vitrimers. However, Li^+ tends to slow down chain diffusion by interacting with the polymer matrix, which leads to a larger increase in τ. This slowing effect becomes even more pronounced as the temperature decreases. As a result, τ (at elevated temperatures) and τ_0 become smaller, but their temperature dependence becomes stronger (larger E_a values) with larger anions.

The characteristic relaxation times τ of imine vitrimers with different anions are plotted as a function of the normalized temperature T_g/T (Figure 2d). Interestingly, all vitrimers exhibited similar τ values at elevated temperatures regardless of anion types. This indicates that bond exchange kinetics is the dominant factor for relaxation behavior rather than chain diffusion and salt dissociation, and additional free catalytic Li ions do not continue to accelerate exchange. The picture of bond exchange being controlling relaxation at high temperatures has been reported in several prior neutral vitrimer studies.[73−75] Supporting this view, Sing et al. recently showed that a segregation of timescale between segmental dynamics and bond exchange kinetics can reach up to six orders of magnitude at high temperatures.[72] However, deviations began to appear upon cooling, where chain diffusion and salt dissociation increasingly contribute to relaxation dynamics. In contrast, imine vitrimers containing different cations did not show universal trends within the measured temperature range (Figure S13) even with T_g normalization, suggesting that their viscoelastic behavior appears to be dominated by cation-specific catalytic effects on bond exchange. This is because catalytic effects become stronger with smaller cation sizes, significantly influencing relaxation behaviors beyond segmental chain dynamics.

Stress relaxation experiments were performed to probe terminal relaxation behavior at low temperatures. Notably, the terminal relaxation behavior of the imine vitrimers cannot be fully described by a single-mode Maxwell model (Figure S13), suggesting that our vitrimers exhibit slower relaxation than Maxwellian behavior at longer timescales. This slower decay may arise from a distribution of relaxation modes. This variance has been observed in previous works, which reported that the Kohlrausch−Williams−Watts (KWW) model can more accurately capture this behavior in vitrimer systems.[69−71] Thus, we employed the KWW stretched exponential equation to fit our data, which yielded a better fit compared to the single Maxwell mode. in the KWW model, the data act more like a Maxwell model as a stretch parameter β approaches to 1. It is worth noting that the β value of neutral vitrimers is smaller than most salt-containing vitrimers, indicating a broader distribution of relaxation modes. An exception was observed in LiBr vitrimers, which showed the β value, even smaller than the neutral sample. We hypothesize that this exception may arise from catalytic effects of cations on bond exchange kinetics, mainly dominating relaxation behavior. In the case of LiBr vitrimers, strong association (Br^--PEO) and high salt dissociation energy may introduce additional heterogeneity into relaxation modes, leading to even smaller β than the neutral vitrimers. The characteristic relaxation times τ obtained from the KWW fitting were plotted in an Arrhenius plot to determine E (Figure S15). The trends in τ and E_a for different ions were found to be mostly consistent with frequency sweep experiment results (Table S3). It is worth noting that τ for neutral and some salt vitrimers (e.g., KTFSI and ImTFSI) crossed at low temperatures, suggesting that the salt-added vitrimers can exhibit slower relaxation than the neutral vitrimer

https://doi.org/10.1021/acs.chemmater.5c00991
Chem. Mater. 2025, 37, 7037−7048

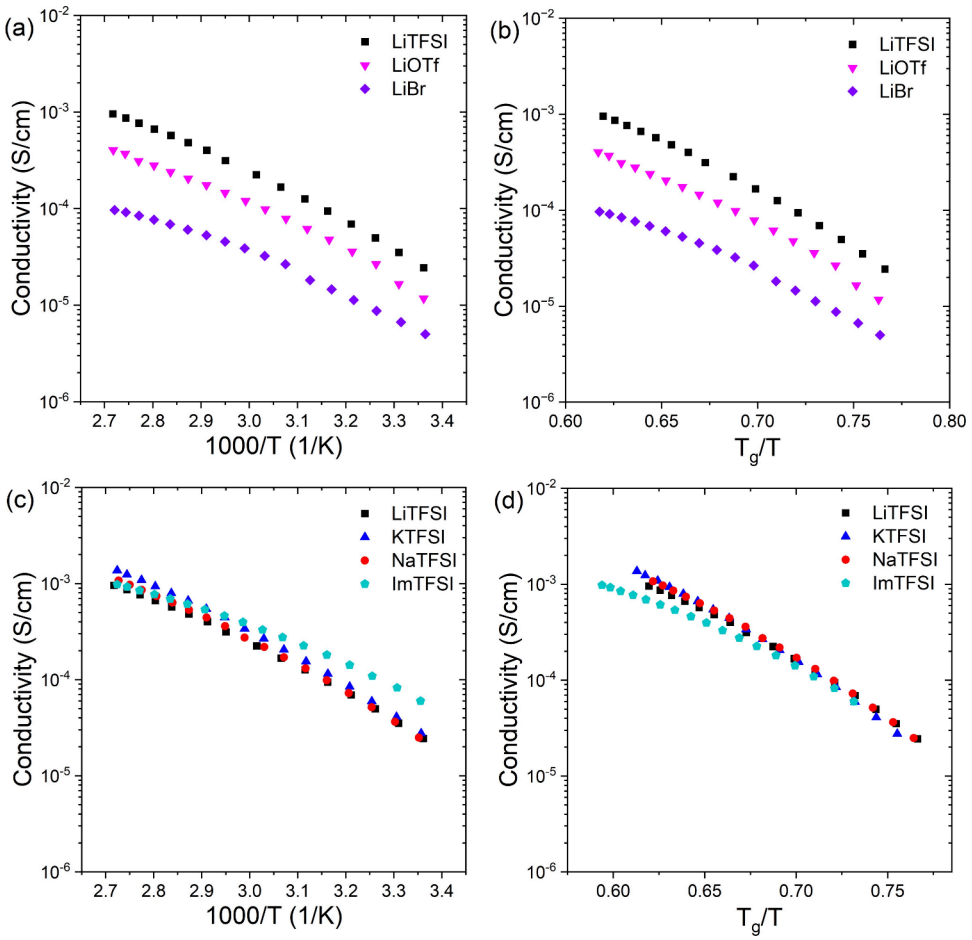

Figure 4. Ionic conductivities of vitrimers with different anions but the same cation as a function of (a) $1000/T$ and (b) T_g/T. Ionic conductivities decreased with smaller anions due to their low degree of ion dissociation. Ionic conductivities of vitrimers with different cations but the same anion as a function of (c) $1000/T$ and (d) T_g/T. Similar ionic conductivities are observed regardless of cation and data converging after normalization, indicating that segmental dynamics primarily govern ionic charge transport.

at low temperatures, where restricted chain diffusion by ion−polymer interactions significantly outweighs catalyzed bond exchanges.

Effect of Different Salts on Morphology of Imine Vitrimers. Wide-angle X-ray scattering (WAXS) was used to characterize the microstructure of the imine vitrimers. WAXS patterns of vitrimers with four different cations (Li^+, Na^+, K^+, and Im^+) and the same anion ($TFSI^-$) were compared to the neutral vitrimer (Figure 3a). The neutral vitrimer showed two distinct peaks at 13.4 and 16.3 nm^{-1}, corresponding to the crystallization of PEO chains.[57] However, after salt addition, these peaks disappeared or were significantly suppressed. A broad amorphous halo peak around 14 nm^{-1} appeared instead, arising from the plasticizing effect of TFSI anions. Imine vitrimers with Li^+, Na^+, and K^+ also showed an additional peak around 9 nm^{-1}, which is attributed to anion−anion correlation.[30,31,56,60−62] Meanwhile, the sample with imidazolium cations did not exhibit this peak. Conversely, LiOTf and LiBr retained crystalline peaks at 13.4 and 16.3 nm^{-1}, though they were less pronounced than those of the neutral vitrimer (Figure 3b). This behavior is due to their smaller anion sizes and reduced ion dissociation, leading to a less effective plasticizing effect. It is worth mentioning that LiOTf and LiBr vitrimers exhibited relatively sharp peaks around 8.4 and 9.3 nm^{-1}, respectively. Those peaks could result from stronger anion−anion correlation as observed from cation vitrimers.

Characteristic values of the shear modulus were determined from the rubbery plateau regime from linear viscoelastic oscillatory shear experiments at a frequency of 10 rad/s (Figure S17). All salt-containing vitrimers except the LiBr system exhibited a smaller shear modulus than the neutral vitrimer due to the plasticizing effect of TFSI and OTf anions. The LiBr vitrimer showed a higher shear modulus than the neutral vitrimer. This observation may result from stronger associations between bromide ions and PEO chains,[36] leading to reduced chain mobility. Moreover, the shear modulus increased with temperature in all vitrimer samples except for LiBr vitrimers, which is attributed to the nearly constant cross-linking density of vitrimers with associative bond exchange mechanisms.[28] On the other hand, the shear modulus for the LiBr vitrimer sample did not exhibit significant temperature dependence, which may arise from ionic interactions that are dissociative.

Effect of Different Salts on Ionic Conductivity of Imine Vitrimers. Electrochemical impedance spectroscopy (EIS) was used to measure the ionic conductivity of the imine salt vitrimers across a temperature range between 25 and 95 °C (Figure S18). The ionic conductivity generally ranged between 10^{-6} and 10^{-4} S/cm at 25 °C. First, vitrimer samples with various anions (Br^-, OTf^-, and $TFSI^-$) and the same cation (Li^+) were measured (Figure 4a). Prior studies reported that the degree of salt dissociation decreased with smaller anions

https://doi.org/10.1021/acs.chemmater.5c00991
Chem. Mater. 2025, 37, 7037−7048

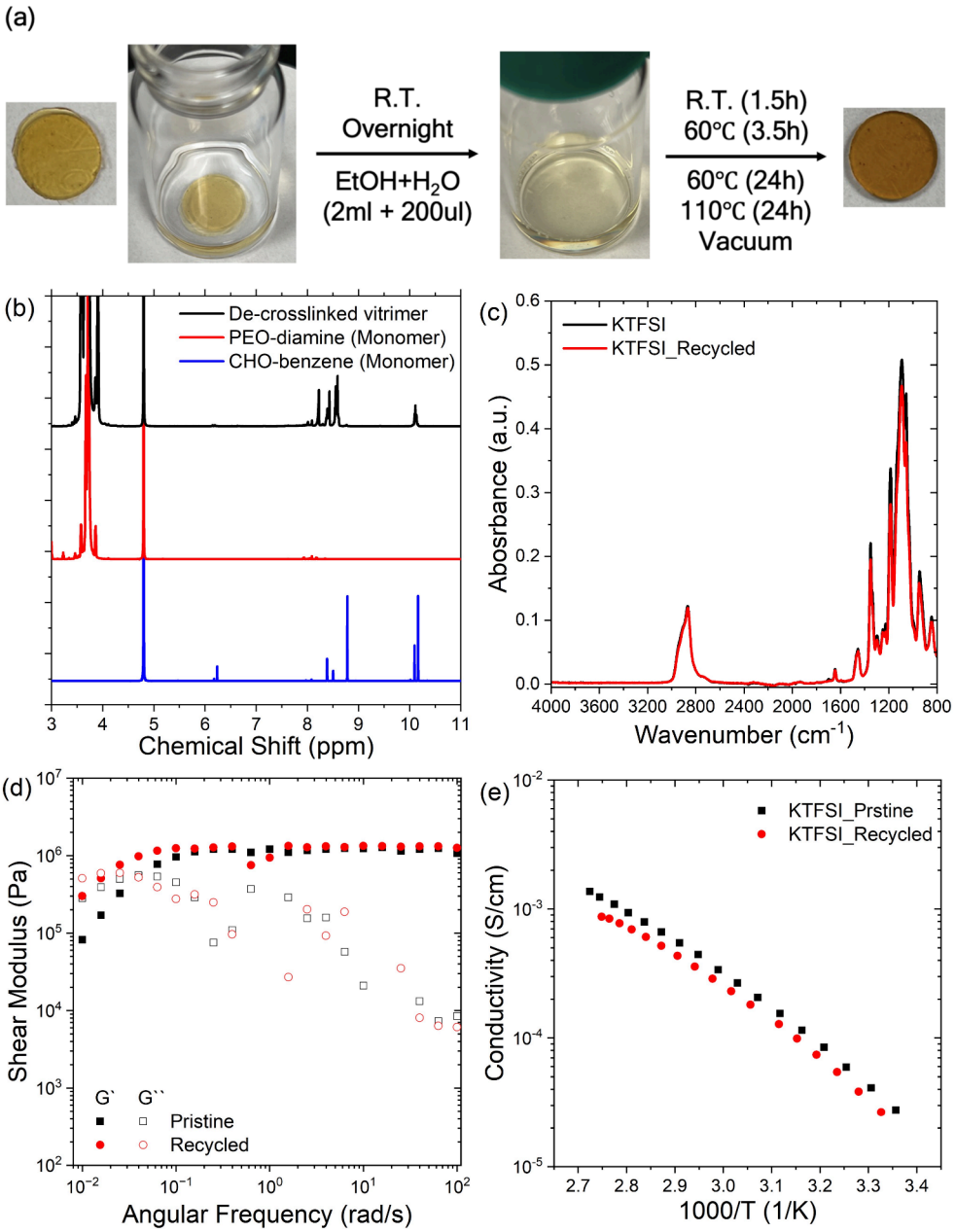

Figure 5. Reprocessability and recyclability of vitrimers. (a) Schematic of the recycling procedure with sample images. (b) ^{1}H solution NMR spectra in D_2O, showing that the vitrimer with KTFSI salts was completely decomposed into a monomer. (c) ATR-FTIR spectra of pristine and recycled KTFSI salt vitrimers. No degradation or side reactions were observed after recycling. (d) Linear viscoelastic shear oscillatory frequency sweep experiments at 130 °C. The characteristic relaxation time τ increased after recycling, indicating a loss of KTFSI salts. (e) Temperature-dependent ionic conductivities of imine vitrimers with KTFSI salts were measured over a temperature range of 95−25 °C in 5 °C intervals. The ionic conductivity decreased after recycling, suggesting that KTFSI salts were partially lost.

(Table S1).[31,35,54,63−65] As a result, ionic conductivity increases as the anion size increases due to the higher degree of salt dissociation. LiTFSI salts require the lowest salt dissociation energy, resulting in more mobile charge carriers and the highest ionic conductivity. In the T_g-normalized conductivity plot (Figure 4b), the ionic conductivities of different anion vitrimers do not superimpose, indicating a decoupling from the segmental dynamics of polymer backbones. These observations could arise from the different extent of dissociated anions, which serve as the primary charge carriers rather than cations, significantly influencing ion transport beyond segmental dynamics.

The ionic conductivities of vitrimers with variable cations (Li^+, Na^+, K^+, and Im^+) and the same anion ($TFSI^-$) were also characterized (Figure 4c). The non-normalized conductivities are similar for vitrimer samples with Li^+, Na^+, and K^+ but are enhanced for Im^+ at lower temperatures. The differences observed for samples with Im^+ may arise from its larger size and lower charge density, resulting in promoted salt dissociation and corresponding increases in ionic conductivity compared to other alkali metal cations. Upon normalizing absolute temperature values with T_g, the conductivities of cation vitrimers converge into a single curve, suggesting that segmental dynamics primarily govern ion transport (Figure 4d).

https://doi.org/10.1021/acs.chemmater.5c00991
Chem. Mater. 2025, 37, 7037−7048

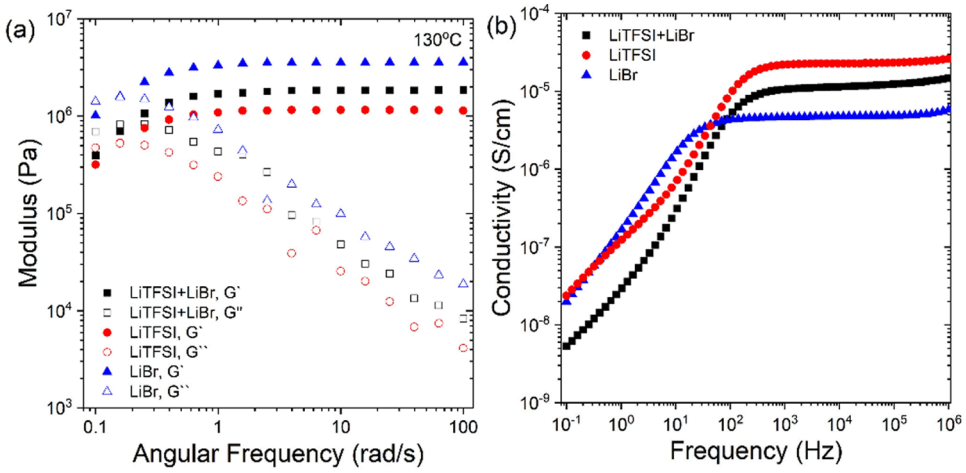

Figure 6. Imine vitrimers with LiTFSI (r = 0.05), LiBr (r = 0.05), and LiTFSI+LiBr (r = 0.025, respectively) salts were analyzed using (a) linear viscoelastic shear oscillatory frequency sweep experiments at 130 °C and (b) ionic conductivity measurements at 25 °C.

Reprocessability, Recyclability, and Tunability of Imine Vitrimers. Previous studies have demonstrated the reprocessability of imine vitrimers by breaking and pressing them.[38−40] In this work, the neutral and salt vitrimers were successfully reprocessed using both thermal and solvent methods. First, the thermal reprocessing method was demonstrated by breaking samples into small pieces and hot pressing them into smooth films. The reprocessed samples showed no notable changes in their TGA, ATR-FTIR, and DSC profiles (Figure S20), indicating no significant degradation during reprocessing. Complete decross-linking was achieved via the solvent method, dissolving KTFSI-containing imine vitrimer films into a mixture of ethanol (2 mL) and water (0.2 mL) by stirring overnight at room temperature. The vitrimer completely dissolved and was readily repolymerized once the solvent was removed (Figure 5a). The complete dissolution of the vitrimer back to a monomer was confirmed using solution ^{1}H NMR in deuterated water (Figure 5b), suggesting that a small amount of water is sufficient to hydrolyze imine bonds and fully decompose the polymer network. The recovery of the vitrimer was achieved by evaporating the solvent. Although the color of the sample changed from yellow to brown, which could be attributed to the oxidation of primary amines during recycling, there was no significant difference in ATR-FTIR and TGA results after recycling (Figure 5c and Figure S19a). However, the characteristic relaxation time τ at 130 °C increased after recycling (Figure 5d), and the sample exhibited lower ionic conductivity than the pristine sample (Figure 5e). The appearance of cold crystallization and melting peak was also observed in the recycled sample (Figure S18b). These changes may result from the loss of KTFSI salt during the recycling process, leading to a reduced catalytic effect from potassium cations, diminished plasticizing effects from TFSI anions, and a lower concentration of ionic charge carriers in the polymers. Although each monomer was not completely separated and purified from the vitrimer-dissolved solution, the monomers were able to be recovered via liquid−liquid extraction, dialysis, and precipitation. Ma and co-workers demonstrated a closed-loop recycling of vinylogous urethane vitrimers.[76] Further optimization of recycling procedures is needed to determine benign solvents and processing conditions to minimize the loss of salts.

Addition of salt influences the rheological properties as well as the ionic conductivity in vitrimer samples. In our prior work, increasing salt concentration in boronic ester vitrimers led to reduced bulk relaxation times and modulus, whereas ionic conductivity increased.[31] Zhou and co-workers found that different alkaline metal salts resulted in distinct stress relaxation behavior and moduli in vinylogous urethane vitrimers.[29] Motivated by these studies, multiple different salts (LiTFSI and LiBr) were added into a single vitrimer sample to modulate the mechanical properties and ionic conductivity. The concentration of each salt was fixed as $r = \frac{[Li^+]}{[EO]} = 0.025$, resulting in the same total concentration as in the single salt vitrimers. High conversion of the polymerization and thermal stability up to 300 °C were confirmed through ATR-FTIR and TGA (Figure S20a,b). The shear storage modulus G' and characteristic relaxation times τ of the mixed salt vitrimers were found to be intermediate to those of the pristine LiTFSI and LiBr vitrimers (Figure 6a). Similarly, the ionic conductivity of the mixed system was intermediate to the pure salt analogs (Figure 6b). The mixed systems were reprocessed successfully up to five times using a hot press by applying a 3-ton pressure at 130 °C for 20 min, maintaining the original shear modulus and ionic conductivity (Figure S21). Overall, these findings suggest that incorporating multiple salts can be a key design principle for controlling the viscoelasticity and ionic conductivity of vitrimers.

CONCLUSIONS

In this work, the effects of different salts on the linear viscoelasticity, morphology, and ionic conductivity of imine vitrimers were investigated. Salt-containing vitrimers exhibited faster relaxation behavior compared to the neutral vitrimers at elevated temperatures, which is attributed to the catalytic effect of cations on imine bond exchange via acting as Lewis acid catalysts. Characteristic relaxation times τ decreased with smaller cations due to their stronger Lewis acidity and enhanced catalytic effects. In contrast, smaller anions result in larger τ, arising from their higher salt dissociation energies, which reduce free cations for catalyzing bond exchange dynamics. The activation energy E also varied with ion size, explained by the combined contribution of chain diffusion, bond exchange kinetics, and salt dissociation. Smaller cations

https://doi.org/10.1021/acs.chemmater.5c00991
Chem. Mater. 2025, 37, 7037−7048

strongly coordinate with polymer chains due to their higher charge densities. This strong interaction hinders chain diffusion, especially at low temperatures, leading to higher E_a. Conversely, larger anions, which require lower salt dissociation energy, promote greater ion dissociation and enhance their interactions with polymer chains. These enhanced interactions further impede chain diffusion particularly at low temperatures, resulting in higher E_a. Li cation vitrimers with various anions exhibit an overlap of relaxation times at elevated temperature upon T_g normalization, but diverge at lower temperatures. This suggests that bond exchange kinetics dominates at elevated temperatures, whereas chain diffusion and salt dissociation increasingly contribute upon cooling, leading to the divergence. In addition, $TFSI^-$ anion vitrimers containing different cations do not converge in the measured temperature window, indicating that the size-dependent catalytic effects of cations on bond exchange primarily govern relaxation behavior rather than segmental dynamics. Our results indicate that several factors, including bond exchange kinetics, chain diffusion, and salt dissociation energy, need to be considered to explain the effect of ions on the viscoelasticity of the vitrimers.

The morphology of vitrimers, analyzed by WAXS, was predominantly influenced by anions. Larger anions, such as TFSI, can plasticize PEO chains and reduce crystallinity. Interestingly, LiBr-containing vitrimers exhibited a higher shear modulus than neutral vitrimers due to the strong association between bromide ions and PEO chains. Ionic conductivity increased with larger anion salts due to their lower salt dissociation energy, which promotes ion dissociation and increases the concentration of charge carriers. Although the conductivity of imine vitrimers with different anions but the same cation is not coupled with segmental dynamics, imine vitrimers with different cations but the same anion exhibited superimposed conductivities governed by segmental dynamics. This contradiction may arise from anions that serve as main ionic charge carriers. These findings highlight the critical role of anions in determining the morphology and ionic conductivity of imine vitrimer electrolytes.

The reprocessability and recyclability of the vitrimers were also demonstrated. The vitrimers could be fully decomposed in a mixture of ethanol and water and recovered by removal of solvent. In addition, the recycled vitrimer retained the initial mechanical properties and ionic conductivity without significant degradation. Finally, mixed salt vitrimers were prepared to show that their viscoelasticity, ionic conductivity, and thermal properties can be tuned by combining multiple salts. The modulus and ionic conductivity of these mixed salt trimers were found to be intermediate between those of the single salt trimers. These results highlight the potential of incorporating multiple salts as a design strategy for vitrimer electrolytes. Overall, this work provides insights into the role of salts on the viscoelastic, thermal, morphological, and ion conductivity properties of imine vitrimers, offering a route for the design and development of recyclable polymer electrolytes.

■ ASSOCIATED CONTENT

Supporting Information

The Supporting Information is available free of charge at https://pubs.acs.org/doi/10.1021/acs.chemmater.5c00991.

Sample photographs, attenuated total reflectance-Fourier transform infrared (ATR-FTIR) spectra, differential calorimetry scanning (DSC) curves, thermogravimetric analysis (TGA), rheometer, ionic conductivity measured by electrochemical impedance spectroscopy (EIS), rheological characterization as a function of temperature (stress relaxation, frequency sweep, and fitting parameter summary table), and storage modulus as a function of temperature (PDF)

■ AUTHOR INFORMATION

Corresponding Author

Christopher M. Evans − *Department of Materials Science and Engineering, Materials Research Laboratory, and Department of Chemical and Biomolecular Engineering, University of Illinois at Urbana−Champaign, Urbana, Illinois 61801, United States;* orcid.org/0000-0003-0668-2500; Email: cme365@illinois.edu

Authors

Seongon Jang − *Department of Materials Science and Engineering, Materials Research Laboratory, and Beckman Institute for Advanced Science and Technology, University of Illinois at Urbana−Champaign, Urbana, Illinois 61801, United States*

Ruey-Bin Tsai − *Department of Materials Science and Engineering, University of Illinois at Urbana−Champaign, Urbana, Illinois 61801, United States*

Charles M. Schroeder − *Department of Materials Science and Engineering, Materials Research Laboratory, Beckman Institute for Advanced Science and Technology, and Department of Chemical and Biomolecular Engineering, University of Illinois at Urbana−Champaign, Urbana, Illinois 61801, United States;* orcid.org/0000-0001-6023-2274

Complete contact information is available at: https://pubs.acs.org/10.1021/acs.chemmater.5c00991

Notes

The authors declare no competing financial interest.

■ ACKNOWLEDGMENTS

The authors gratefully acknowledge the use of research facilities at the Material Research Laboratory (for TGA and DSC), Beckman Institute for Advanced Science and Technology, and School of Chemical Sciences NMR Laboratory (for solution NMR) at the University of Illinois at Urbana−Champaign. This project was supported by the Air Force Office of Scientific Research, Organic Materials Chemistry Program (grant FA-9550-20-1-0262, rheological analysis and characterization), the Department of Energy, Basic Energy Sciences, Materials Chemistry Program (Award DE-SC0020858, ion transport in vitrimers) and the National Science Foundation (NSF) via the Molecular Maker Lab Institute (Award 201987, NSF AI Institute, molecular design).

■ REFERENCES

(1) Sharmili, N.; Nagi, R.; Wang, P. A Review of Research in the Li-Ion Battery Production and Reverse Supply Chains. *J. Energy Storage* **2023**, *68*, No. 107622.

(2) Kim, T.; Song, W.; Son, D.-Y.; Ono, L. K.; Qi, Y. Lithium-Ion Batteries: Outlook on Present, Future, and Hybridized Technologies. *J. Mater. Chem. A* **2019**, *7*, 2942−2964.

(3) Xu, K. Electrolytes and Interphases in Li-Ion Batteries and Beyond. *Chem. Rev.* **2014**, *114* (23), 11503−11618.

(4) Ye, L.; Li, X. A Dynamic Stability Design Strategy for Lithium Metal Solid State Batteries. *Nature* **2021**, *593*, 218−222.
(5) Moradi, Z.; Lanjan, A.; Tyagi, R.; Srinivasan, S. Review on Current State, Challenges, and Potential Solutions in Solid-State Batteries Research. *J. Energy Storage* **2023**, *73*, No. 109048.
(6) Guo, Y.; Qu, X.; Hu, Z.; Zhu, J.; Niu, W.; Liu, X. Highly Elastic and Mechanically Robust Polymer Electrolytes with High Ionic Conductivity and Adhesiveness for High-Performance Lithium Metal Batteries. *J. Mater. Chem. A* **2021**, *9*, 13597−13607.
(7) Wan, J.; Xie, J.; Kong, X.; Liu, Z.; Liu, K.; Shi, F.; Pei, A.; Chen, H.; Chen, W.; Chen, J.; Zhang, X.; Zong, L.; Wang, J.; Chen, L.-Q.; Qin, J.; Cui, Y. Ultrathin, Flexible, Solid Polymer Composite Electrolyte Enabled with Aligned Nanoporous Host for Lithium Batteries. *Nat. Nanotechnol.* **2019**, *14*, 705−711.
(8) Hasan, N.; Pulst, M.; Samiullah, M. H.; Kressler, J. Comparison of Li^+-Ion Conductivity in Linear and Crosslinked Poly(ethylene oxide). *J. Polym. Sci., Part B: Polym. Phys.* **2019**, *57*, 21−28.
(9) Timachova, K.; Watanabe, H.; Balsara, N. P. Effect of Molecular Weight and Salt Concentration on Ion Transport and the Transference Number in Polymer Electrolytes. *Macromolecules* **2015**, *48*, 7882−7888.
(10) Platen, K.; Langer, F.; Bayer, R.; Hollmann, R.; Schwenzel, J.; Busse, M. Influence of Molecular Weight and Lithium Bis-(trifluoromethanesulfonyl)imide on the Thermal Processability of Poly(ethylene oxide) for Solid-State Electrolytes. *Polymers* **2023**, *15*, 3375.
(11) Khurana, R.; Schaefer, J. L.; Archer, L. A.; Coates, G. W. Suppression of Lithium Dendrite Growth Using Cross-Linked Polyethylene/Poly(ethylene oxide) Electrolytes: A New Approach for Practical Lithium-Metal Polymer Batteries. *J. Am. Chem. Soc.* **2014**, *136*, 7395−7402.
(12) Lehmann, M. L.; Yang, G.; Nanda, J.; Saito, T. Well-designed Crosslinked Polymer Electrolyte Enables High Ionic Conductivity and Enhanced Salt Solvation. *J. Electrochem. Soc.* **2020**, *167*, No. 070539.
(13) Fenton, D. E.; Parker, J. M.; Wright, P. V. Complexes of Alkali Metal Ions with Poly(ethylene oxide). *Polymer* **1973**, *14*, 589.
(14) Shriver, D. F.; Papke, B. L.; Ratner, M. A.; Dupon, R.; Wong, T.; Brodwin, M. Structure and Ion Transport in Polymer-Salt Complexes. *Solid State Ionics* **1981**, *5*, 83−88.
(15) Ciaccia, M.; Di Stefano, S. Mechanisms of Imine Exchange Reactions in Organic Solvents. *Org. Biomol. Chem.* **2015**, *13*, 646.
(16) Isogai, T.; Hayashi, M. A Simple Design of a Vitrimer Network with Various Fractions of Bond Exchangeable Units for Revisiting the Arrhenius Dependence of Relaxation Properties. *Polym. Chem.* **2024**, *15*, 269.
(17) Cheng, L.; Zhao, X.; Zhao, J.; Liu, S.; Yu, W. Structure and Dynamics of Associative Exchange Dynamic Polymer Networks. *Macromolecules* **2022**, *55*, 6598−6608.
(18) Spiesschaert, Y.; Taplan, C.; Stricker, L.; Guerre, M.; Winne, J. M.; Du Prez, F. E. Influence of the Polymer Matrix on the Viscoelastic Behaviour of Vitrimers. *Polym. Chem.* **2020**, *11*, 5377.
(19) Krishna Kumar, B.; Dickens, T. J. Dynamic Bond Exchangeable Thermoset Vitrimer in 3D-Printing. *J. Appl. Polym. Sci.* **2023**, *140*, No. e53304.
(20) Yan, T.; Jiang, H.; Pang, W.; He, T.; Cheng, M.; Wang, Z.; Li, C.; Sun, S.; Hu, S. Preparation and Self-Healing Properties of Epoxy Vitrimer Materials Based on Imine Bonds. *J. Appl. Polym. Sci.* **2024**, *141*, No. e55684.
(21) Wanasinghe, S. V.; Dodo, O. J.; Konkolewicz, D. Dynamic Bonds: Adaptable Timescales for Responsive Materials. *Angew. Chem., Int. Ed.* **2022**, *61*, No. e202206938.
(22) Yan, P.; Zhao, W.; Zhang, B.; Jiang, L.; Petcher, S.; Smith, J. A.; Parker, D. J.; Cooper, A. I.; Lei, J.; Hasell, T. Inverse Vulcanized Polymers with Shape Memory, Enhanced Mechanical Properties, and Vitrimer Behavior. *Angew. Chem., Int. Ed.* **2020**, *59*, 13371−13378.
(23) Yang, Y.; Terentjev, E. M.; Zhang, Y.; Chen, Q.; Zhao, Y.; Wei, Y.; Ji, Y. Reprocessable Thermoset Soft Actuators. *Angew. Chem., Int. Ed.* **2019**, *58*, 17474−17479.
(24) Yang, Y.; Wang, H.; Zhang, S.; Wei, Y.; He, X.; Wang, J.; Zhang, Y.; Ji, Y. Vitrimer-Based Soft Actuators with Multiple Responsiveness and Self-Healing Ability Triggered by Multiple Stimuli. *Matter* **2021**, *4*, 3354−3365.
(25) Lee, J.; Jing, B. B.; Porath, L. E.; Sottos, N. R.; Evans, C. M. Shock Wave Energy Dissipation in Catalyst-Free Poly-(dimethylsiloxane) Vitrimers. *Macromolecules* **2020**, *53*, 4741−4747.
(26) Cheng, L.; Zhao, J.; Xiong, Z.; Liu, S.; Yan, X.; Yu, W. Hyperbranched Vitrimer for Ultrahigh Energy Dissipation. *Angew. Chem., Int. Ed.* **2024**, *63*, No. e202406937.
(27) Lin, Y.; Chen, Y.; Yu, Z.; Huang, Z.; Lai, J.-C.; Tok, J. B.-H.; Cui, Y.; Bao, Z. Reprocessable and Recyclable Polymer Network Electrolytes via Incorporation of Dynamic Covalent Bonds. *Chem. Mater.* **2022**, *34*, 2393−2399.
(28) Jang, S.; Alvarez, E. I. H.; Chen, C.; Jing, B. B.; Shen, C.; Braun, P. V.; Schleife, A.; Schroeder, C. M.; Evans, C. M. Control of Lithium Salt Partitioning, Coordination, and Solvation in Vitrimer Electrolytes. *Chem. Mater.* **2023**, *35*, 8039−8049.
(29) Liu, J.; Li, J.-J.; Luo, Z.-H.; Zhou, Y.-N. Fast Room-Temperature Self-healing Vitrimers Enabled by Accelerated Associative Exchange Kinetics. *Chem. Eng. J.* **2023**, *452*, No. 139452.
(30) Jing, B. B.; Evans, C. M. Catalyst-Free Dynamic Networks for Recyclable, Self-Healing Solid Polymer Electrolytes. *J. Am. Chem. Soc.* **2019**, *141* (48), 18932−18937.
(31) Jing, B. B.; Mata, P.; Zhao, Q.; Evans, C. M. Effects of Crosslinking Density and Lewis Acidic Sites on Conductivity and Viscoelasticity of Dynamic Network Electrolytes. *J. Polym. Sci.* **2021**, *59* (21), 2492−2501.
(32) Tominaga, Y.; Yamazaki, K.; Nanthana, V. Effect of Anions on Lithium Ion Conduction in Poly(ethylene carbonate)-based Polymer Electrolytes. *ECS Trans.* **2014**, *62* (1), 151−157.
(33) Fragiadakis, D.; Dou, S.; Colby, R. H.; Runt, J. Molecular Mobility, Ion Mobility, and Mobile Ion Concentration in Poly-(ethylene oxide)-Based Polyurethane Ionomers. *Macromolecules* **2008**, *41*, 5723−5728.
(34) Khudyshkina, A. D.; Butzelaar, A. J.; Guo, Y.; Hoffmann, M.; Bergfeldt, T.; Schaller, M.; Indris, S.; Wilhelm, M.; Théato, P.; Jeschull, F. From Lithium to Potassium: Comparison of Cations in Poly(ethylene oxide)-Based Block Copolymer Electrolytes for Solid-State Alkali Metal Batteries. *Electrochim. Acta* **2023**, *454*, No. 142421.
(35) Chen, C.; Mei, B.; Zhou, J.; Schweizer, K. S.; Evans, C. M.; Braun, P. V. Coupling of Ethylene-Oxide-Based Polymeric Network Structure and Counterion Chemistry to Ionic Conductivity and Ion Selectivity. *Macromolecules* **2024**, *57*, 6779−6788.
(36) Stefanovic, R.; Webber, G. B.; Page, A. J. Nanostructure of Propylammonium Nitrate in the Presence of Poly(ethylene oxide) and Halide Salts. *J. Chem. Phys.* **2018**, *148*, No. 193826.
(37) Shen, K.-H.; Hall, L. M. Effect of Ion Size and Dielectric Constant on Ion Transport and Transference Number in Polymer Electrolytes. *Macromolecules* **2020**, *53*, 10086−10096.
(38) Deng, K.; Zhou, S.; Xu, Z.; Xiao, M.; Meng, Y. A High Ion-Conducting, Self-Healing and Nonflammable Polymer Electrolyte with Dynamic Imine Bonds for Dendrite-Free Lithium Metal Batteries. *Chem. Eng. J.* **2022**, *428*, No. 131224.
(39) Xue, X.; Cao, X.; Wan, L.; Tong, Y.; Li, T.; Xie, Y. Crosslinked Network Solid Polymer Electrolyte with Self-Healing Ability and High Stability for Lithium Metal Battery. *Polym. Int.* **2022**, *71* (10), 1201−1209.
(40) Cao, X.; Zhang, P.; Guo, N.; Tong, Y.; Xu, Q.; Zhou, D.; Feng, Z. Self-Healing Solid Polymer Electrolyte Based on Imine Bonds for High Safety and Stable Lithium Metal Batteries. *RSC Adv.* **2021**, *11*, 2985−2994.
(41) Wan, L.; Cao, X.; Xue, X.; Tong, Y.; Ci, S.; Huang, H.; Zhou, D. Self-Healing and Flexible Ionic Gel Polymer Electrolyte Based on Reversible Bond for High-Performance Lithium Metal Batteries. *Energy Technol.* **2021**, *10*, No. 2100749.
(42) Zhang, L.; Zhang, P.; Chang, C.; Guo, W.; Guo, Z. H.; Pu, X. Self-Healing Solid Polymer Electrolytes for Room-Temperature Solid-

https://doi.org/10.1021/acs.chemmater.5c00991
Chem. Mater. 2025, 37, 7037−7048

State Lithium Metal Batteries. *ACS Appl. Mater. Interfaces* **2021**, *13*, 46794−46802.
(43) Zhang, P.; Guo, W.; Guo, Z. H.; Ma, Y.; Gao, L.; Cong, Z.; Zhao, X. J.; Qiao, L.; Pu, X.; Wang, Z. L. Dynamically Crosslinked Dry Ion-Conducting Elastomers for Soft Iontronics. *Adv. Mater.* **2021**, *33*, No. 2101396.
(44) Gu, W.; Li, F.; Liu, T.; Gong, S.; Gao, Q.; Li, J.; Fang, Z. Recyclable, Self-Healing Solid Polymer Electrolytes by Soy Protein-Based Dynamic Network. *Adv. Sci.* **2022**, *9*, No. 2103623.
(45) Yang, S.; Park, S.; Kim, S.; Kim, S.-K. Vitrimer with Dynamic Imine Bonds as a Solid-State Electrolyte for Lithium Metal Batteries. *Mater. Today Energy* **2024**, *45*, No. 101690.
(46) Bandara, T. M. W. J.; Fernando, H. D. N. S.; Furlani, M.; Albinsson, I.; Dissanayake, M. A. K. L.; Ratnasekera, J. L.; Mellander, B.-E. Effect of the Alkaline Cation Size on the Conductivity in Gel Polymer Electrolytes and their Influence on Photo Electrochemical Solar Cells. *Phys. Chem. Chem. Phys.* **2016**, *18*, 10873.
(47) Memboeuf, A.; Vékey, K.; Lendvay, G. Structure and Energetics of Poly(ethylene glycol) Cationized by Li^+, Na^+, K^+ and Cs^+: A First-Principles Study. *Eur. J. Mass Spectrom.* **2011**, *17*, 33−46.
(48) Winne, J. M.; Leibler, L.; Du Prez, F. E. Dynamic Covalent Chemistry in Polymer Networks: A Mechanistic Perspective. *Polym. Chem.* **2019**, *10*, 6091−6108.
(49) Wu, S. L.; Chen, Q. Advances and New Opportunities in the Rheology of Physically and Chemically Reversible Polymers. *Macromolecules* **2022**, *55*, 697−714.
(50) Self, J. L.; Dolinski, N. D.; Zayas, M. S.; de Alaniz, J. R.; Bates, C. M. Brønsted-Acid-Catalyzed Exchange in Polyester Dynamic Covalent Networks. *ACS Macro Lett.* **2018**, *7*, 817−821.
(51) Isogai, T.; Hayashi, M. Critical Effects of Branch Numbers at the Cross-Link Point on the Relaxation Behaviors of Transesterification Vitrimers. *Macromolecules* **2022**, *55*, 6661−6670.
(52) Samanta, S.; Kim, S.; Saito, T.; Sokolov, A. P. Polymers with Dynamic Bonds: Adaptive Functional Materials for a Sustainable Future. *J. Phys. Chem. B* **2021**, *125*, 9389−9401.
(53) Perego, A.; Khabaz, F. Creep and Recovery Behavior of Vitrimers and Fast Bond Exchange Rate. *Macromol. Rapid Commun.* **2023**, *44*, No. 2200313.
(54) Lee, M.; Choi, U. H.; Colby, R. H.; Gibson, H. W. Ion Conduction in Imidazolium Acrylate Ionic Liquids and their Polymers. *Chem. Mater.* **2010**, *22*, 5814−5822.
(55) Oteo, U.; Martinez-Ibañez, M.; Aldalur, I.; Sanchez-Diez, E.; Carrasco, J.; Armand, M.; Zhang, H. Improvement of the Cationic Transport in Polymer Electrolytes with (Difluoromethanesulfonyl)-(trifluoromethanesulfonyl)imide Salts. *ChemElectroChem.* **2019**, *6*, 1019−1022.
(56) Jang, S.; Schroeder, C. M.; Evans, C. M. Multiple Energy Dissipation Modes in Dynamic Polymer Networks with Neutral and Ionic Junctions. *Chem. Commun.* **2024**, *60*, 8431−8434.
(57) Zardalidis, G.; Mars, J.; Allgaier, J.; Mezger, M.; Richter, D.; Floudas, G. Influence of Chain Topology on Polymer Crystallization: Poly(ethylene oxide) (PEO) Rings vs. *Linear Chains. Soft Matter.* **2016**, *12*, 8124−8134.
(58) Carden, G. P.; Martins, M. L.; Toleutay, G.; Cheng, S.; Blad, B.; Foster, J.; Gainaru, C.; Sokolov, A. P. Critical Role of the Steric Factor in the Viscoelasticity of Vitrimers. *Macromolecules* **2025**, *58*, 5494−5504.
(59) He, M.; Leh, J.-M. Metal Cation-Driven Dynamic Covalent Formation of Imine and Hydrazone Ligands Displaying Synergistic Co-catalysis and Auxiliary Amine Effects. *Chem. - Eur. J.* **2021**, *27*, 7516−7524.
(60) Choi, U. H.; Lee, M.; Wang, S.; Liu, W.; Winey, K. I.; Gibson, H. W.; Colby, R. H. Ionic Conduction and Dielectric Response of Poly(imidazolium acrylate) Ionomers. *Macromolecules* **2012**, *45*, 3974−3985.
(61) Choi, U. H.; Ye, Y.; Salas de la Cruz, D.; Liu, W.; Winey, K. I.; Elabd, Y. A.; Runt, J.; Colby, R. H. Dielectric and Viscoelastic Responses of Imidazolium-Based Ionomers with Different Counterions and Side Chain Lengths. *Macromolecules* **2014**, *47*, 777−790.
(62) Zhao, Q.; Shen, C.; Halloran, K. V.; Evans, C. M. Effect of Network Architecture and Linker Polarity on Ion Aggregation and Conductivity in Previse Polymerized Ionic Liquids. *Macromolecules* **2019**, *8*, 658−663.
(63) Kwon, H.; Kim, S.; Park, H.; Park, J. S.; Park, J.; Lee, Y.; Yang, S. J.; Choi, U. H. Enhancing Energy Density in Flexible All-Solid-State Supercapacitors via Dielectricizer Zwitterion-Containing Quasi-Solid-State Polymer Electrolyte. *Adv. Funct. Mater.* **2024**, *34*, No. 2406727.
(64) Song, Z.; Xing, Z.; Yang, J.; Chen, J.; Hu, W.; Li, P.; Feng, W.; Eshetu, G. G.; Figgemeier, E.; Passerini, S.; Armand, M.; Zhou, Z.; Zhang, H. Electrolyte Chemistry Development for Sodium-Based Batteries: A Blueprint from Lithium or a Step Toward Originality? *Angew. Chem., Int. Ed.* **2025**, No. e202424543.
(65) Kim, C. K.; Won, J.; Kim, H. S.; Kang, Y. S.; Li, H. G.; Kim, C. K. Density Functional Theory Studies on the Dissociation Energies of Metallic Salts: Relationship between Lattice and Dissociation Energies. *J. Comput. Chem.* **2001**, *22*, 827−834.
(66) Van Lijsebetten, F.; Maes, S.; Winne, J. M.; Du Prez, F. E. Thermoswitchable Catalysis to Inhibit and Promote Plastic Flow in Vitrimers. *Chem. Sci.* **2024**, *15*, 7061.
(67) Brooks, D. J.; Merinov, B. V.; Goddard, W. A.; Kozinsky, B.; Mailoa, J. Atomistic Description of Ionic Diffusion in PEO-LiTFSI: Effect of Temperature, Molecular Weight, and Ionic Concentration. *Macromolecules* **2018**, *51*, 8987−8995.
(68) Safandowska, M.; Makarewicz, C.; Rozanski, A.; Idczak, R. Barrier Properties of Semicrystalline Polylactide: The Role of the Density of the Amorphous Regions. *Macromolecules* **2022**, *55*, 10077−10089.
(69) Cuminet, F.; Berne, D.; Lemouzy, S.; Dantras, É.; Joly-Duhamel, C.; Caillol, S.; Leclerc, É.; Ladmiral, V. Catalyst-Free Transesterification Vitrimers: Activation via α-difluoroesters. *Polym. Chem.* **2022**, *13*, 2651−2658.
(70) Kimura, T.; Hayashi, M. One-Shot Transformation of Ordinary Polyesters into Vitrimers: Decomposition-Triggered Cross-linking and Assistance of Dynamic Covalent Bonds. *J. Mater. Chem. A* **2022**, *10*, 17406−17414.
(71) Hayashi, M.; Yano, R.; Takasu, A. Synthesis of Amorphous low T_g Polyesters with Multiple COOH Side Groups and their Utilization for Elastomeric Vitirmers Based on Post-Polymerization Cross-linking. *Polym. Chem.* **2019**, *10*, 2047−2056.
(72) Lin, T.-W.; Mei, B.; Dutta, S.; Schweizer, K. S.; Sing, C. E. Molecular Dynamics Simulation and Theoretical Analysis of Structural Relaxation, Bond Exchange Dynamics, and Glass Transition in Vitrimers. *Macromolecules* **2025**, *58*, 1481−1497.
(73) Ge, S.; Evans, C. M. Influence of Segmental Dynamics on Bond Exchange in Imine Vitrimers with Different Polymer Backbones and CrossLinkers. *Macromolecules* **2025**, *58*, 4043−4053.
(74) Xia, J.; de la Cruz, M. O. Effect of Molecular Structure on the Dynamics and Viscoelasticity of Vitrimers. *Polymer* **2024**, *308*, No. 127371.
(75) Wu, J.-B.; et al. Relationship between Reaction Kinetics and Chain Dynamics of Vitrimers Based on Dioxaborolane Metathesis. *Macromolecules* **2020**, *53* (8), 1180−1190.
(76) Ma, Y.; Jiang, X.; Shi, Z.; Berrocal, J. A.; Weder, C. Closed-Loop Recycling of Vinylogous Urethane Vitrimers. *Angew. Chem., Int. Ed.* **2023**, *62* (36), No. e202306188.

https://doi.org/10.1021/acs.chemmater.5c00991
Chem. Mater. 2025, 37, 7037−7048